PHYSICAL REVIEW B VOLUME 57, NUMBER 19 15 MAY 1998-I

Giant magnetoresistance in zero-band-gap $Hg_{1-x}Cd_xTe$

Tineke Thio,* S. A. Solin, J. W. Bennett, and D. R. Hines
NEC Research Institute, 4 Independence Way, Princeton, New Jersey 08540

M. Kawano, N. Oda, and M. Sano
Material Development Center, NEC Corporation, 1-1, Miyazaki 4-chome, Miyamae-ku, Kawasaki, Kanagawa 216, Japan

(Received 8 January 1998)

The exceptionally high carrier mobilities found in zero-gap $Hg_{1-x}Cd_xTe$ ($x \approx 0.10$) give rise to giant magnetoresistance (GMR). A two-carrier, high-field model provides a good description of the magnetoresistance and Hall effect at temperatures $6<T<300$ K and magnetic fields up to $H=10$ T. The high-field data have a significant influence on the interpretation of the low-field results, in particular revealing the presence of acceptors despite the fact that the low-field Hall coefficient is negative. Surprisingly, at low fields the curvature of the GMR, d^2R/dH^2, is larger than that expected by up to a factor 30. The enhancement of the GMR makes $Hg_{1-x}Cd_xTe$ potentially useful for read-head devices for magnetic media. [S0163-1829(98)09419-3]

I. INTRODUCTION

Solid solutions of mercury cadmium telluride with composition $Hg_{1-x}Cd_xTe$ have been extensively investigated during the past 30 years.[1,2] The interest in these materials to date derives primarily from the compositional dependence of their band gap, which makes them useful as both emitters and detectors of photons with a selectable characteristic wavelength.[3,4] In particular, $Hg_{1-x}Cd_xTe$ with $x \approx 0.2$ is marketed commercially as a detector for the industrially important infrared region at wavelengths of ~ 10 μm.[5] Moreover, $Hg_{1-x}Cd_xTe$ is a rich model system in which to explore the basic physics of bulk and lower-dimensional narrow- and zero-gap semiconductors.[6] Such explorations usually focus on the very high electron mobilities exhibited by $Hg_{1-x}Cd_xTe$ in the zero-gap ($x \approx 0.10$) composition region.

The majority of the studies of $Hg_{1-x}Cd_xTe$ to date have been carried out on bulk single crystals, although some results have been reported on thin-film materials. Typically, $Hg_{1-x}Cd_xTe$ is electrically characterized by measuring the low-field magnetotransport properties as a function of temperature and composition, with the carrier mobility serving as a *de facto* figure of merit.[7,8] However, in this work we show that in order to account properly for the low-field galvanomagnetic behavior of $Hg_{1-x}Cd_xTe$ one must also take into account the high-field behavior. We report high-field magnetoresistance (MR) and Hall effect measurements on molecular-beam epitaxy (MBE) grown $Hg_{1-x}Cd_xTe$ with $x \approx 0.10$. The experiments, done over the range $6<T<300$ K and at magnetic fields up to $H=10$ T, indicate that single-carrier models found commonly in the literature[7,9–11] are inadequate for the interpretation of the data at high fields and low temperatures. However, as we demonstrate in this paper, an elegant picture emerges from a two-band model, which includes both electrons and holes: $Hg_{1-x}Cd_xTe$ ($x \approx 0.10$) is a zero-band-gap semiconductor, of which the electron density follows a power law $n_0(T)=A_nT^{3/2}$; at low temperature acceptors are evident with a density that exceeds the donor density by $N_A-N_D=3.5\times10^{22}$ m^{-3}. We observe high electron mobility $\mu_e \approx 10$ m^2/V s; the hole mobility is much smaller, with $\mu_e/\mu_h \approx 200$.

Because of the high electron mobility, the MR of $Hg_{1-x}Cd_xTe$ is indeed properly characterized as ''giant'' (hence GMR) at high fields. Surprisingly, at the magnetic fields relevant in magnetic media ($H<1000$ G), the GMR is anomalously large, with the low-field curvature d^2R/dH^2 exceeding that at high field by up to a factor 30. The use of the Corbino geometry[12] further boosts the response; in such a sample we have observed GMR as large as $\Delta\rho/\rho=28\%$ at $T=300$ K and $H=500$ G. This material therefore has significant potential for applications in MR-based devices for high-density magnetic data storage and retrieval and may have qualities superior to those of spin valves[13] for use as read heads for magnetic storage media.

II. EXPERIMENTAL DETAILS

The $Hg_{1-x}Cd_xTe$ films studied were grown by conventional MBE methods using a Riber 32P MBE system.[14] Onto single-crystal Si substrates were deposited a 4-μm buffer layer of undoped CdTe followed by the $Hg_{1-x}Cd_xTe$ layer of thickness $d=4.6$ μm. The sample composition was determined to be $x=0.10$ with an accuracy of $\Delta x=\pm0.015$, using energy dispersive x-ray analysis with a $Hg_{0.78}Cd_{0.22}Te$ standard. The samples used in this study were undoped and unannealed. They were determined to be homogeneous on a length scale of 3 mm, to within the accuracy of the measurement.[15]

Magnetotransport measurements were done in both the Hall bar and Corbino geometries;[12] in the latter geometry the current and voltage leads are concentric circles. Electrical contact was made to the samples by evaporating pure In in lithographically defined patterns as illustrated in the insets of Fig. 1. The six-probe Hall geometry (8×3 mm^2) allows the simultaneous measurement of the Hall voltage and the magnetoresistance. The effect of the geometry on the measurements will be discussed in Sec. IV. Copper wires were attached to the In contacts using conductive silver paint (Dupont No. 4929N). The contacts were found to be Ohmic

0163-1829/98/57(19)/12239(6)/$15.00 © 1998 The American Physical Society

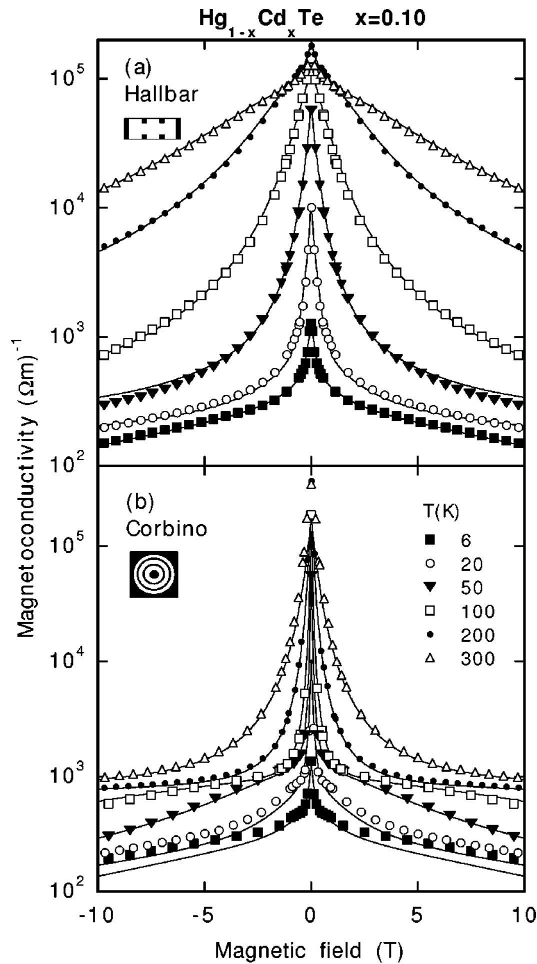

FIG. 1. Magnetoconductivity $\sigma(H)$ in (a) Hall bar and (b) Corbino disk, at the temperatures indicated. Symbols indicate selected data and solid lines are fits.

down to $T=4$ K; nevertheless, all the resistance measurements were done in a four-probe configuration in order to eliminate any effects of contact and lead resistance. The samples were placed on a temperature-controlled sample holder, in the center of an Oxford superconducting magnet. H is applied perpendicular to the film. Automated data taking, including temperature regulation and reading and magnetic field sweeps, was accomplished with LabView software.

III. RESULTS

The magnetoconductivity $\sigma(H)$ is shown in Fig. 1 for the Hall bar [Fig. 1(a)] and Corbino [Fig. 1(b)] geometries at selected temperatures as indicated in the legend. In this figure, as in Figs. 2 and 4, for clarity only selected data points are shown, by symbols; the solid lines indicate fits to the model described in Sec. IV. The MR, defined as $\Delta\rho(H)/\rho_0 = [\rho(H)-\rho(0)]/\rho_0$, is positive at all temperatures and rises quadratically with field at small H (see Fig. 2). For $T \geq 100$ K, the MR is quadratic at high magnetic fields as well, but with a curvature d^2R/dH^2, which is smaller than that at low field by up to a factor ≈ 20. In Fig. 1, a geometric factor distinguishes the MR measured in the Hall bar sample and in the Corbino disk:[12,16,17] In the former a measurement

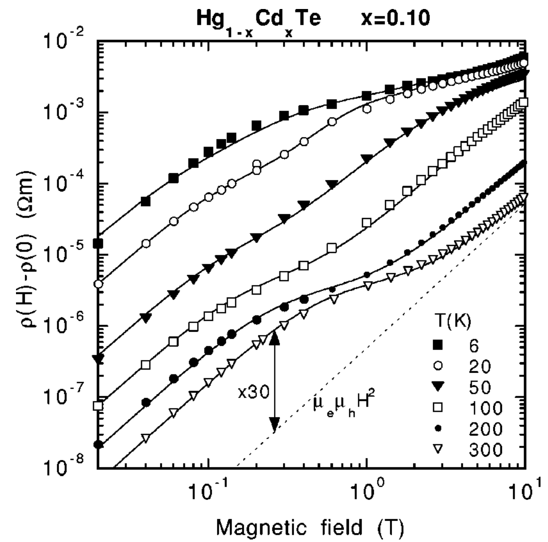

FIG. 2. Magnetoresistance $\rho(H)-\rho(0)$ in the Hall bar on a log-log plot.

of the resistance gives the resistivity $1/ne\mu_e$ in the case of extrinsic conduction, whereas the Corbino disk resistance gives $(1+\mu_e^2H^2)/ne\mu_e$. This is also evident in the difference between the temperature dependences of the MR at various fields, as shown in Fig. 3: The Corbino MR is significantly larger than the Hall bar MR for $T>100$ K; how-

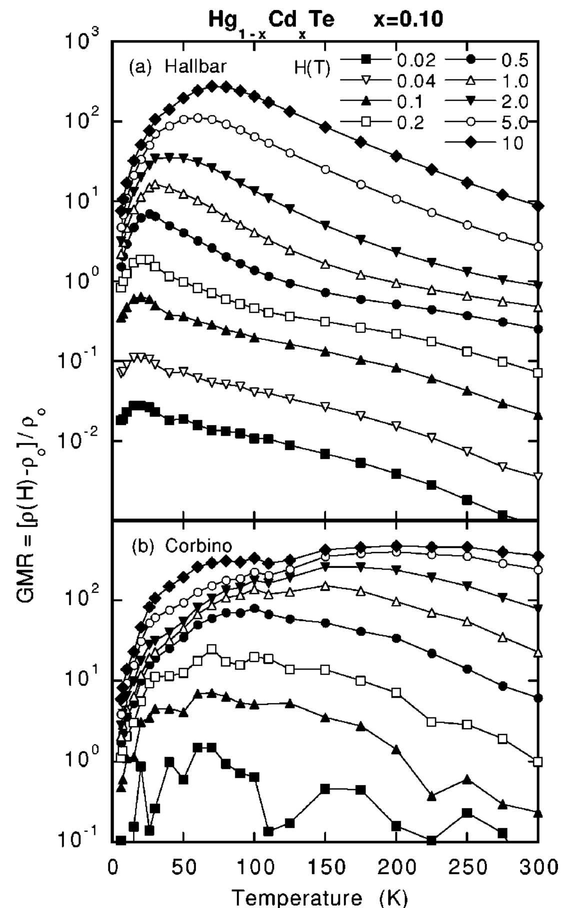

FIG. 3. Temperature dependence of $\rho(H)/\rho(0)$ in (a) Hall bar and (b) Corbino disk, at the fields indicated. The solid lines are guides to the eye.

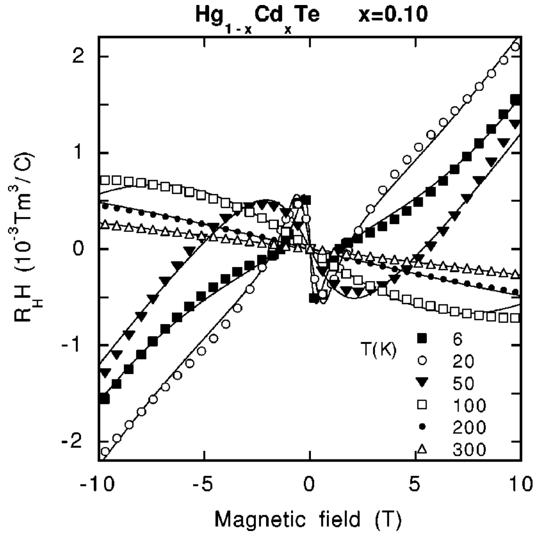

FIG. 4. Field dependence of the Hall voltage at selected temperatures. Symbols indicate selected data and solid lines are fits.

ever, at low temperature the MR's in the two geometries are comparable. The complexity of the MR is reflected in the temperature and magnetic-field-dependent Hall coefficient R_H, which exhibits a rich behavior; see Fig. 4, where the Hall voltage $V_y \sim R_H H$ is plotted as a function of field, at temperatures corresponding to those shown in Fig. 1. For $T \geqslant 100$ K, R_H is negative, indicating n-type conduction (see the discussion below on the low-field behavior). For $T < 100$ K, $V_y(H)$ is highly nonlinear and shows a crossover from n-type conduction at low field to p-type conduction at high magnetic field. The temperature dependence of the low-field Hall voltage ($H = 0.1T$) is consistent with that reported in the literature;[7,9–11,18] however, as the following discussion shows, the high-field data have a significant influence on the interpretation of the low-field results. The temperature dependence of the zero-field conductivity, measured in the Hall bar geometry, is shown in Fig. 5; $\sigma_{HB}(H=0;T)$ increases slightly on cooling from room temperature, reaches a maximum, and decreases sharply on further cooling.

IV. DISCUSSION

From the data of Figs. 1–3 it is clear that $Hg_{1-x}Cd_xTe$ indeed shows giant magnetoresistance: The GMR is as large as $\Delta\rho(H)/\rho_0 = 275$ at $H = 10$ T and $T \approx 75$ K. The temperature dependence of $\sigma_{HB}(T)$ (Fig. 5) and the maximum in $\Delta\rho(H)/\rho(0)$ (Fig. 3) suggest that the dominant transport mechanism at low temperature is different from that at high temperature. A similar crossover occurs in the Hall effect (Fig. 4). We now discuss the details of the magnetotransport to address these features.

Since $Hg_{1-x}Cd_xTe$ with $x = 0.10$ is close to the zero-band-gap composition,[1] both electrons and holes are expected to contribute to the transport properties. We therefore use a two-band model for the magnetoconductivity and the Hall coefficient. Furthermore, since the electron mobilities are very high, the high-field limit $\mu_e H > 1$ is reached at relatively small fields; for this reason we use a model that is appropriate at both low and high fields:[17,19]

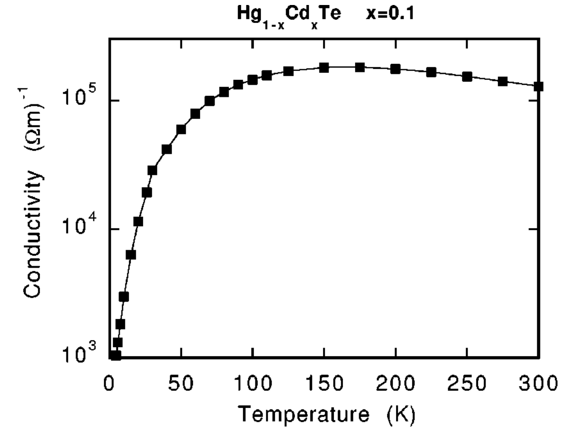

FIG. 5. Temperature dependence of zero-field conductivity (in the Hall bar). The solid line is a guide to the eye.

$$\sigma_{HB}(H) = \sum_c \sigma_{Hc} \left[1 + \left(\frac{\sum_c \sigma_{Hc}\mu_{Hc}}{\sum_c \sigma_{Hc}} \right)^2 H^2 \right], \quad (1)$$

$$\sigma_{Corb}(H) = \sum_c \sigma_{Hc}, \quad (2)$$

$$R_H(H) = \frac{\sum_c \sigma_{Hc}\mu_{Hc}}{\left(\sum_c \sigma_{Hc}\right)^2 \left[1 + \left(\frac{\sum_c \sigma_{Hc}\mu_{Hc}}{\sum_c \sigma_{Hc}} \right)^2 H^2 \right]}, \quad (3)$$

where σ_{HB} and σ_{Corb} denote the effective conductivities measured in Hall bar and Corbino geometries, respectively. The index c denotes the electrons and holes; $\sigma_{Hc} = N_c e \mu_{Hc}/(1 + \mu_{Hc}^2 H^2)$ and $\mu_{Hc} = \mathrm{sgn}(q_c)\mu_H$, the Hall mobility modified by the sign of the carrier. Equations (1)–(3) reduce to the usual low-field ($\mu_H H < 1$) expressions when $H = 0$, namely, $\sigma_{HB} = \sigma_{Corb} = ne\mu_e + pe\mu_h$ and $R_H = (pe\mu_h^2 - ne\mu_e^2)/(pe\mu_h + ne\mu_e)^2$.

In fitting the model to the data, we adopt the simplest possible field dependence for the carrier densities (n,p) and mobilities (μ_e, μ_h), which are consistent with the data as well as with a reasonable physical picture for a zero-band-gap semiconductor. The assumption of a field-independent electron mobility $\mu_e(H) = \mu_{e0}$ gives a good fit at high H, but fails to describe adequately the low-field data where the magnetoconductance has a higher curvature than at high H (see Fig. 2). We assume that at high temperature the electron density is independent of the field and assign the anomalously enhanced conductivity at zero field to an enhancement of the electron mobility, which decreases quadratically with field. For the purpose of fitting to the data, we use a Lorentzian form in order to disallow negative mobilities at high H; the complete expression for the electron mobility is thus $\mu_e(H) = \mu_{e0} + A/(B + H^2)$. A similar expression is required

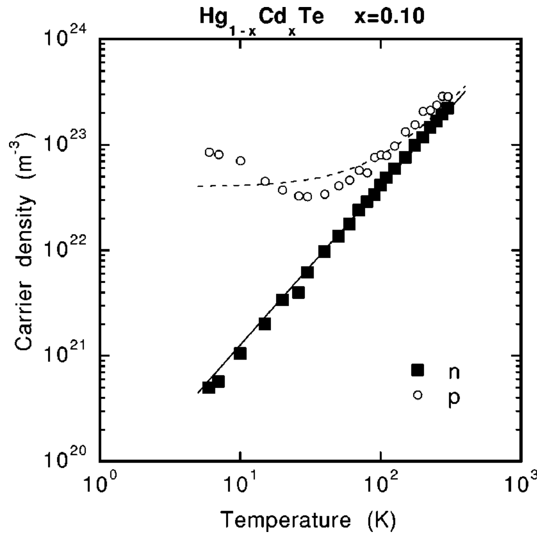

FIG. 6. Carrier density at $H=0$: electrons $n_0(T)$ (solid circles) and holes $p_0(T)$ (open circles). The solid line shows $n_0(T)=A_nT^{3/2}$ and the dotted line shows $p_0(T)=n_0(T)+N_A$.

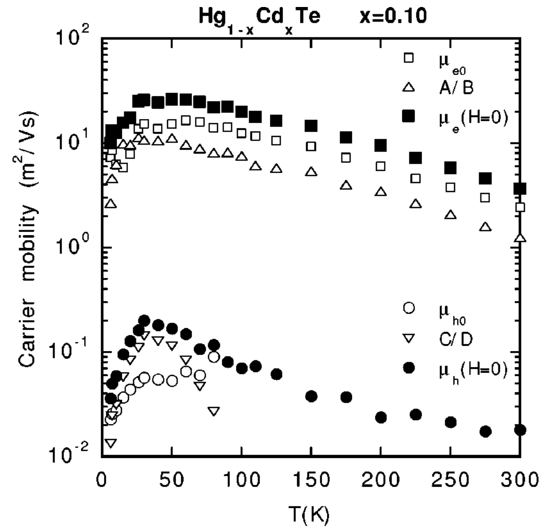

FIG. 7. High-field carrier mobility for electrons (open squares) and holes (open circles) and their zero-field enhancement A/B (triangles) and C/D (inverted triangles); total zero-field mobilities $\mu_e(H=0)=\mu_{e0}+A/B$ (solid squares) and $\mu_h(H=0)=\mu_{h0}+C/D$ (solid circles).

for the hole mobility in order to fit the data at all temperatures and magnetic fields consistently.

The external magnetic field is expected to induce a finite gap given by the cyclotron frequency $E_g=\hbar\omega_c=\hbar eH/m^*$ (SI units). The electron density is therefore expected to decrease with field, following (to lowest order) a quadratic field dependence, also expressed as a Lorentzian with width H_n: $n(H)=n_0/(1+H^2/H_n^2)$. This approximation is sufficient at high temperature (indeed we find that H_n becomes much larger than 10 T for $T>200$ K). At low temperatures and high field one expects $n(H)$ to decrease exponentially with H; however, at high field the transport properties are dominated by holes to such an extent that the electron contribution is not apparent in the data at all. In this regime, the MR does show that the hole density decreases with the applied field.

The field dependences of the carrier densities used in fitting the data to the model are summarized as

$$n(H)=\frac{n_0}{1+H^2/H_n^2},$$

$$p(H)=p_0\exp(-QH) \tag{4}$$

and for the carrier mobilities

$$\mu_e(H)=\mu_{e0}+\frac{A}{B+H^2},$$

$$\mu_h(H)=\mu_{h0}+\frac{C}{D+H^2}. \tag{5}$$

The Hall bars are rather short and wide, which introduces a reduction of the measured Hall voltage by a geometrical factor G: $V_{y,meas}=GV_y$.[17] For a length-to-width ratio $l/w=2.7$ and with the Hall voltage probes positioned about 30% along the length of the sample, $G>90\%$, so the uncertainty in the fitting parameters from the geometrical effect is less than 10%. Moreover, the correction vanishes at high magnetic fields, at which the Hall angle becomes large (which is satisfied for $\mu_H H>1$, or $H>0.1$ T for the electrons).

The model described by Eqs. (1)–(5) is fit to the MR and Hall effect data taken in the Hall bar geometry. The fits, denoted in Figs. 1, 2, and 4 by solid lines, show that the model yields an excellent fit to both the MR and the Hall effect data over the entire field and temperature range of the measurement, including at low temperatures, where the Hall voltage has a complex field dependence. The solid lines of Fig. 1(b) show the MR in the Corbino disk predicted from the fitting parameters obtained from the Hall bar. The prediction shows very good agreement with the data, except at low fields; we will return to this issue below. The fitting parameters, which yield the temperature dependence of the carrier densities and mobilities, are all derived from the Hall bar data.

The zero-field carrier concentrations are shown in Fig. 6. The electron concentration follows a power-law temperature dependence $n_0(T)=A_nT^{3/2}$; this is exactly what is expected for a zero-gap semiconductor with parabolic bands;[1] the power law is obeyed over nearly three orders of magnitude, with $A_n=4.0\times10^{19}$ m^{-3} K$^{-3/2}$. At low T, however, $p_0(T)$ saturates, indicating a density of acceptors $N_A=(3.5\pm1)\times10^{22}$ m^{-3} in this nominally undoped material. The increase of $p_0(T)$ at the lowest temperatures is likely to be an artifact since $p(H)$ in this region is fitted to an exponential in H [see Eq. (4)]; if saturation occurs at low H, the prefactor p_0 is an overestimate of the actual hole density at $H=0$. At all temperatures, $p_0(T)=n_0(T)+N_A$, as required by the charge neutrality condition. The origin of the acceptors may be residual vacancies on the (Cd,Hg) sites.[20] Elimination of such vacancies requires a postgrowth annealing in a Cd or Hg atmosphere, whereas the samples studied here are unannealed. Alternatively, acceptors may arise from vacancies on the Te site, which have recently been found to form a double

acceptor state instead of the usually expected double donor state, due to a lattice relaxation in the local environment of the Te vacancy.[21]

The temperature dependences of the carrier mobilities are summarized in Fig. 7, which shows the high-field mobilities μ_{e0} and μ_{h0}, the zero-field enhancements A/B and C/D for electron and hole mobilities, respectively, and the total zero-field mobilities. For the electrons, the zero-field enhancement is apparent at all temperatures, but for the holes the width of the zero-field effect (given by the parameter D) becomes comparable to the range of the measurement close to $T=70$ K; above that temperature the data contain no information on the zero-field enhancement for the hole mobility. The assumption that any such enhancement becomes very small at $T>70$ K (that is, $\mu_{h0}=\mu_{h,tot}$) is consistent with the fact that the total hole mobility shows no abrupt changes around $T=70$ K. The high-field electron mobility is indeed very high, reaching nearly 20 m^2/V s at intermediate temperatures. Both μ_{e0} and μ_{h0} decrease at high temperature, consistent with electron-phonon scattering[10] and $\mu_e/\mu_h \approx 200$, in agreement with results found in the literature.[1]

In the context of the data of Figs. 6 and 7, the temperature dependence of the zero-field conductivity can be interpreted as follows. At high temperature, $n_0 \approx p_0$, but the conductivity is dominated by the electrons, which have a much higher mobility than the holes; in this region $\sigma_{HB}(T)$ has a weak temperature dependence (see Fig. 5) because of the competing effects of the decreasing electron mobility and the increasing electron density. For $T<100$ K, a low-field measurement of the Hall effect suggests[9–11] that the decrease of $\sigma_{HB}(T)$ results from a decrease in the electron mobility $\mu_e(T)$. However, the data of Figs. 6 and 7 show that this is not the case; rather, since $p_0 \gg n_0$ for $T<100$ K, the hole contribution to the transport properties becomes significant, despite the fact that $\mu_e \gg \mu_h$ in this region. It is the low hole mobility that causes the decrease of $\sigma_{HB}(T)$ at low temperature.

The above confirms the importance of taking into account the high-field data as well as using a two-band model: In Fig. 6, the power law $n_0(T) \sim T^s$ with $s=3/2$ is obeyed over nearly three orders of magnitude; however, when only low-field ($H \leq 0.1$ T) data are considered, a one-band model yields $n_0(T)$, which shows curvature on a log-log plot. This may explain why the exponent s has been reported[22] to vary between 1.45 and 2.3. Furthermore, the negative Hall effect observed at low temperatures (and low field) is commonly attributed to the presence of donors. In contrast, in the above we have shown that if donors are present, their density is lower than that of the acceptors.

From the prefactor $A_n=4.0\times10^{19}$ m^{-3} $K^{-3/2}$ (see Fig. 6) and the ratio of the carrier mobilities $\mu_{e0}/\mu_{h0} \approx 200$, it is straightforward to estimate the electron and hole effective masses. We find $m_e^*/m_0=0.012$ and $m_h^*/m_0=2.5$; the former is consistent with the values quoted for $Hg_{1-x}Cd_xTe$ by Dornhaus and Nimtz,[1] $m_e^*/m_0=0.008$ at $n\approx10^{22}$ m^{-3} and $m_e^*/m_0=0.016$ at $n\approx10^{23}$ m^{-3} at the critical value of x, for which the band gap $E_g=0$ ($x_c\approx0.15$ at $T=4$ K).

The quadratic field dependence of the MR seen at high field and high temperature (see Fig. 2) is a consequence of the material being close to the intrinsic limit. In the case $n=p$,[19,23] Eq. (1) reduces to $\Delta\rho/\rho_0=\mu_e\mu_h H^2$. This relation is valid at all magnetic fields; it is therefore surprising that at low field the curvature of the MR is larger than $\mu_e\mu_h$ by up to a factor 30. For an extrinsic and nondegenerate electron gas, appropriate for the densities measured here, the electron scattering gives rise[23] to a MR that for $\mu_e H<1$ has the form $\Delta\rho/\rho_0=T_M\mu_e H^2$, where T_M is of order unity. Although for the material reported here the MR curvature at low field has a similar temperature dependence as μ_e^2,[24] the relation is not expected to be valid in the intrinsic limit attained at high temperatures; furthermore, in n-type doped samples[25] the MR curvature does not have the same temperature dependence as μ_e^2. Further studies of this enhancement of the GMR in the technologically relevant field range are under way.

We now discuss the field dependence of the carrier concentration at low temperature. For $T\leq50$ K, at high field the conductivity is dominated by holes and $p(H)$ fits a form [see Eq. (3)] exponential in the magnetic field: $p(H)=p_0\exp(-QH)$. This is consistent with the opening of the band gap by the application of the magnetic field. Since the temperature dependence of p_0 indicates the presence of acceptors, we identify $p(H,T)=p_0(T)\exp[-E_b(H)/kT]$, where E_b is the hydrogenic binding energy of an acceptor impurity, which is expected to scale with the band gap (ignoring corrections due to the changing effective mass). From the temperature dependence of $Q(T)$, we find $E_b/H=45$ μeV/T; a binding energy of $E_b=0.45$ meV at $H=10$ T is consistent with the fact that the exponential high-field behavior is observed only at the lowest temperatures.

The dominance of acceptors at low T and high H prevents the direct measurement of the band gap, but an impurity binding energy of 0.45 meV at $H=10$ T is entirely consistent with a band gap $E_g=\hbar\omega_c=97$ meV at that field. Such a gap is not apparent in the technologically relevant region around room temperature, where the electron concentration is independent of field (Fig. 4) and has the temperature dependence of a zero-gap semiconductor (Fig. 6). One path towards obtaining a finite effect due to the opening of a gap is the use of truly zero-gap material at low temperature ($x_c\approx0.15$ at $T=4$ K),[26] but at very low carrier densities, requiring annealed, undoped $Hg_{1-x}Cd_xTe$ in which the acceptor concentration is minimized. In this case the carrier effective mass is very small, leading to a divergence of the cyclotron frequency. Under these conditions the band gap is most sensitive to the applied magnetic field.

The use of a Corbino[12] geometry can be used to further increase the GMR (see Fig. 3). The MR measured in such a sample is larger than that measured in a Hall bar by a factor $1+\mu^2H^2$.[16,17] This is a significant factor since the electron mobilities in $Hg_{1-x}Cd_xTe$ are very high. Indeed, in a Corbino disk of $Hg_{1-x}Cd_xTe$ we have measured a room-temperature GMR of $\Delta\rho/\rho=28\%$ at $H=500$ G. The highest carrier mobilities have been reported in samples with $x=x_c$ and at low carrier densities.[1] Since both the field-induced band gap and the use of the Corbino geometry favor $Hg_{1-x}Cd_xTe$ at the critical concentration and low density, further explorations of such materials will be important for GMR-based read-head applications.

V. CONCLUSION

Measurements of the magnetotransport in $Hg_{1-x}Cd_xTe$ ($x \approx 0.10$) are well described by a two-carrier model. The data are consistent with an interpretation based on a zero-band-gap semiconductor, with $n_0(T) = A_n T^{3/2}$. Residual acceptors are evident at $T < 100$ K, with a density $N_A = 3.5 \times 10^{22}$ m^{-3}, and a binding energy that rises approximately linearly in H and is found to be $E_b = 0.45$ meV at $H = 10$ T. The electron mobility is very high ($\mu_e \approx 10$ $m^2/V\,s$ and $\mu_e/\mu_h \approx 200-300$) and gives rise to GMR that at high field is well described by the conventional relation $\Delta\rho/\rho_0 = \mu_e \mu_h H^2$. Surprisingly, however, at low field the curvature of the GMR is larger by up to a factor 30. The use of the Corbino geometry further boosts the response to an external magnetic field. The large size of the low-field GMR makes $Hg_{1-x}Cd_xTe$ an excellent candidate for MR-based heads for high-density data storage and retrieval.

---

*Electronic address: tineke@research.nj.nec.com

[1] R. Dornhaus and G. Nimtz, *Narrow-Gap Semiconductors*, Springer Tracts in Modern Physics Vol. 98 (Springer-Verlag, New York, 1983), p. 119 ff.

[2] W.E. Tennant, C.A. Cockrum, J.B. Gilpin, M.Z. Kinch, M.B. Reine, and R.P. Ruth, J. Vac. Sci. Technol. B **10**, 1359 (1992).

[3] P.W. Kruse, in *Semiconductors and Semimetals, Vol. 18, Mercury Cadmium Telluride*, edited by R.K. Willardson and A.C. Beer (Academic Press, San Diego, 1981).

[4] M.B. Reine, P.W. Norton, R. Starr, M.H. Weiler, M. Kestigian, B.L. Musicant, P. Mitra, T. Schimert, F.C. Case, I.B. Bhat, H. Ehsani, and V. Rao, J. Electron. Mater. **24**, 669 (1995).

[5] M.J. Bevan (private communication).

[6] L. Ghenim, R.G. Mani, J.R. Anderson, and J.T. Cheung, Solid State Commun. **75**, 341 (1990).

[7] J.S. Kim, D.G. Seiler, R.A. Lancaster, and M.B. Reine, J. Electron. Mater. **25**, 1215 (1996).

[8] W.M. Higgins, G.N. Pultz, R.G. Roy, R.A. Lancaster, and J.L. Schmit, J. Vac. Sci. Technol. A **7**, 271 (1989).

[9] L.N. Korol', L.A. Bovina, and V.I. Stafeev, Fiz. Tekh. Poluprovodn. **11**, 498 (1977) [Sov. Phys. Semicond. **11**, 288 (1977)]; L.N. Korol', V.S. Vershinin, L.A. Bovina, and V.I. Stafeev, *ibid.* **12**, 476 (1978) [*ibid.* **12**, 275 (1978)].

[10] J.J. Dubowski, T. Dietl, W. Szymanska, and R.R. Galazka, J. Phys. Chem. Solids **42**, 351 (1981).

[11] S. Sone, N. Oda, T. Sasaki, and M. Kawano, J. Cryst. Growth **117**, 218 (1992).

[12] O.M. Corbino, Phys. Z. **12**, 561 (1911).

[13] D.J. Monsma, J.C. Lodder, Th.J.A. Popma, and B. Dieny, Phys. Rev. Lett. **74**, 5260 (1995).

[14] M. Kawano, A. Ajisawa, N. Oda, M. Nagashima, and H. Wada, Appl. Phys. Lett. **69**, 2876 (1996).

[15] S.A. Solin, Tineke Thio, D.R. Hines, J.W. Bennett, M. Kawano, M. Oda, and N. Sano, Appl. Phys. Lett. **69**, 4105 (1996).

[16] R.S. Popovic, *Hall Effect Devices* (IOP Publishing Ltd., Bristol, 1991).

[17] R.S. Allgaier, Semicond. Sci. Technol. **3**, 306 (1988).

[18] N.N. Berchenko, A.S. Zakhar'yash, I.I. Izhnin, S.P. Komissarchuk, and M.V. Pashkovskii, Fiz. Tekh. Poluprovodn. **13**, 1030 (1979) [Sov. Phys. Semicond. **13**, 602 (1979)].

[19] R.A. Smith, *Semiconductors* (Cambridge University Press, Cambridge, 1959).

[20] R. Krause-Rehberg, Th. Drost, and A. Polity, Mater. Sci. Forum **143-147**, 429 (1994); D.M. Hofmann, P. Omling, H.G. Grimmeiss, D. Sinerius, K.W. Benz, and B.K. Meyer, *ibid.* **83-87**, 1235 (1992).

[21] D.J. Chadi (unpublished).

[22] C. Verié, Phys. Status Solidi **17**, 889 (1966).

[23] K. Seeger, *Semiconductor Physics*, 5th ed. (Springer-Verlag, Berlin, 1991).

[24] T. Thio, S.A. Solin, J.W. Bennett. D.R. Hines, M. Kawano, N. Oda, and M. Sano (unpublished).

[25] T. Thio, S.A. Solin, J.W. Bennett, D.R. Hines, M. Kawano, N. Oda, and M. Sano, J. Cryst. Growth **184-185**, 1293 (1998).

[26] G.L. Hansen, J.L. Schmit, and T.N. Casselman, J. Appl. Phys. **53**, 7099 (1982).